CFD-based design and analysis of the ventilation of an electric generator model, validated with experiments

Citation for the original published paper (version of record):
Jamshidi, H., Nilsson, H., Chernoray, V. (2015). CFD-based design and analysis of the ventilation of an electric generator model, validated with
experiments. International Journal of Fluid Machinery and Systems, 8(2): 113-123.
http://dx.doi.org/10.5293/IJFMS.2015.8.2.113

International Journal of Fluid Machinery and Systems
Vol. 8, No. 2, April-June 2015

DOI: http://dx.doi.org/10.5293/IJFMS.2015.8.2.113
ISSN (Online): 1882-9554

Original Paper

CFD-based Design and Analysis of the Ventilation of an Electric Generator Model, Validated with Experiments

Hamed Jamshidi[1], Håkan Nilsson[1] and Valery Chernoray[1]

[1] Chalmers University of Technology
Göteborg, 412 96, Sweden, hamed.jamshidi@chalmers.se

Abstract

The efficiency of the ventilation system is a key point for durable and reliable electric generators. The design of such system requires a detailed understanding of the air flow in the generator. Computational fluid dynamics (CFD) has the potential to resolve the lack of information in this field. The present work analyses the air flow inside a generator model. The model is designed using a CFD-based approach, and manufactured by taking into consideration the experimental and numerical requirements and limitations. The emphasis is on the possibility to accurately predict and experimentally measure the flow distribution inside the stator channels. A major part of the work is focused on the design of an intake and a fan that gives an evenly distributed flow with a high flow rate. The intake also serves as an accurate flowmeter. Experimental results are presented, of the total volume flow rate, the total pressure and velocity distributions. Steady-state CFD simulations are performed using the FOAM-extend CFD toolbox. The simulations are based on the multiple rotating reference frames method. The results from the frozen rotor and mixing plane rotor-stator coupling approaches are compared. It is shown that the fan design provides a sufficient flow rate for the stator channels, which is not the case without the fan or with a previous fan design. The detailed experimental and numerical results show an excellent agreement, proving that the results reliable.

Keywords: Experiments, CFD, Electric Generator and Ventilation.

1. Introduction

The heat that is generated by losses in electric generators is most commonly removed by a forced air flow, to keep the temperature limited and uniform. The primary purposes of a generator cooling system is to provide adequate cooling for the insulation materials and limit the thermal stresses within acceptable levels. A well-designed cooling system thus assures lower operation and maintenance costs. The ventilation of electric generators occurs through the empty spaces of the rotor and the stator, see Fig. 1. A stator consists of stator windings and a stator core. The stator windings convert the mechanical energy to electrical energy by an interaction with the rotating magnetic flux provided by the rotor. These stator windings are recessed in and supported by the slots formed by the assembly of the laminated core. The core is comprised of a stack of thin iron plates. Each plate has a thin coating of insulation. Spacers are located between some plate layers, to form channel passages for the flow of cooling air. The rotor assembly consists of structural parts, and poles with exciting windings. In salient pole machines, there is an inter-polar space that allows for the flow of cooling air. There are often axial and/or centrifugal fan blades mounted on the rotor to increase the flow rate. Sometimes there may be external fans to further increase the flow rate, when necessary. A sufficient total air flow rate is essential to ensure that the flow is adequate in every stator cooling channel and that it is uniformly distributed. Improvements of the air flow properties lead both to a more uniform cooling in time and space, and to an improvement of the overall efficiency of the machine due to decreased windage losses.

The process of conversion of the mechanical energy into electricity in generators includes three main classes of energy losses [1], electric losses, magnetic losses and mechanical losses. Electric losses are due to the electric resistance in the stator coils and other conductors. Magnetic losses appear as a result of the rotating magnetic field. The mechanical losses are mainly caused by the flow of cooling air (windage loss), and friction in bearings. All these losses eventually generate heat, which raises the temperature of the machine components and induces an undesirable change in the material properties. High or varying temperatures may reduce the efficiency and affect the lifetime of

Received June 1 2015; accepted for publication June 25 2015:
Corresponding author: Hamed Jamshidi, PhD Student, hamed.jamshidi@chalmers.se

This paper was presented at the 27th IAHR Symposium on Hydraulic Machinery and Systems, September 4, Montreal, Canada.

certain components, such as insulation, and thus increase the maintenance requirements of the generator. It is therefore important to remove the heat to keep the generator at a stable, uniform, and limited temperature, while keeping the windage losses to a minimum. Improvements in ventilation and cooling methods increase the generator life expectancy and offer means to run the machines at higher rating without any major investments and modifications in the structures.

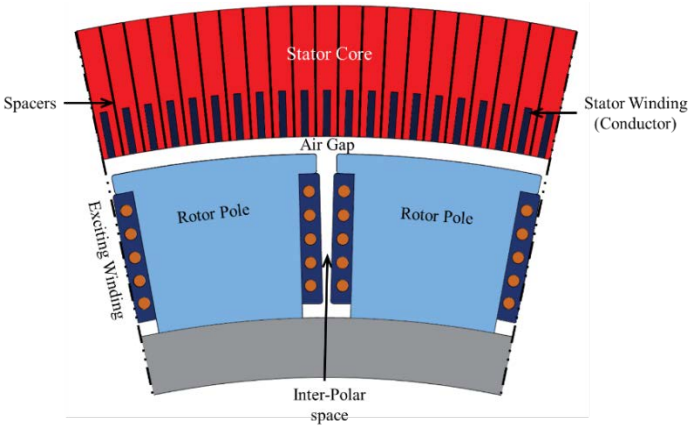

Fig. 1 A schematic cross-section of a two-pole sector of an electric generator.

Numerical ventilation studies and thermal simulations of electric generators can be divided into two main categories, thermal networks and Computational Fluid Dynamics (CFD) [2]. The thermal network approach has the ability to analyze large and complex systems very fast. The design process of the convective cooling of electrical machines is primarily based on this method. The accuracy of the network method is however strongly dependent on the underlying empirical thermal parameters, in particular the convective heat transfer correlations. In most cases, experimental data must be used to calibrate the thermal network models in order to get sufficiently accurate results. Overall, the heat transfer at the end windings or the flow field inside the stator ducts can barely be computed using thermal networks, while the application of three-dimensional numerical methods makes these predictions possible. CFD offers a good potential to fully predict ventilation and cooling in generators [2-16]. CFD has the advantage that it can be used to predict the flow and heat transfer in complex regions, without case-specific empirical correlations. Accurate CFD results can be used for improving the thermal network correlations without the need of costly experiments. However, the designers need to have confidence in the use of CFD, so more research must be done to validate the CFD modeling results.

There are few available scientific CFD studies performed on the flow of cooling air in electric generators. Pickering et al. [3] summarized the results of research work to validate the CFD modeling of large salient pole machines. It was concluded that CFD can be used to provide valuable insight into the air flow and heat transfer in salient pole machines, which in turn can aid the machine design. Shanel et al. [4] investigated the heat transfer and ventilation of an air-cooled generator by using a general purpose CFD code in a simplified generator design. They concluded that CFD analysis can be used effectively to predict temperatures in electrical machines by combining conduction heat transfer with airflow and convective heat transfer modeling. Ujiie et al. [5] demonstrated that CFD is a valuable addition to the network method for the design optimization of electrical machines, if the accuracy is confirmed in a model test. The validated CFD procedures could be used as a standalone tool to compute flow, heat transfer, temperatures and even windage losses. Toussaint et al. [7] presented 2D and 3D simulation strategies to numerically compute the flow field in electric generators. Their 2D calculations showed that the steady-state multiple frames of reference solution is sensitive to the type (frozen rotor vs. mixing plane) and location of the rotor-stator interface (RSI). However, their 3D simulations showed that the relative flow distributions are unaffected by changes in the RSI configuration. Pasha et al. [8] did experimental and CFD analysis on a partial model of stator. They observed that major losses occur in the wedge zone and leading edge of the windings. Schrittwieser et al. [9] presented an analysis of the fluid flow in the stator ducts of a hydro generator using CFD. They conclude that the leading side of the stator slot has a better heat exchange than the trailing side. Zhang et al. [10] simulated the flow field of a dual radial ventilation system without a fan, for a hydro-generator. Their study showed that the local pressure loss of the stator entrance is dominant. They mentioned that a rational design of the stator duct entrances can both reduce the pressure loss of the stator ventilation, and improve the cooling in the stator ducts. Moradnia et al. [11-13] performed steady-state frozen rotor simulations of a simplified electric generator and validated the results with experimental measurements. They developed a fully predictive simulation method for a hydro-generator model. Klomberg et al. [14, 15] investigated different methods of analyzing a large hydro generator with computational fluid dynamics, using two transient and two steady-state approaches. Their studies focused on the end winding area and the influence of different ventilation schemes on heat transfer and fluid flow.

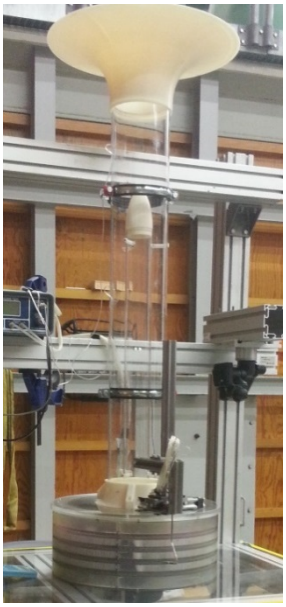

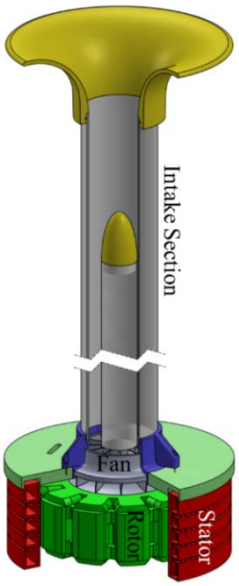

Fig. 2 Left: Modified generator model. Right: Main parts of modified generator model.

The current study aims at attaining a better phenomenological understanding, and more accurate predictions, of the ventilation airflow in electric generators. The work is based on both experimental and numerical studies of an electric generator model that is specifically designed for the purpose of ventilation studies. Geometrical design modifications are introduced, to get a higher mass flow and better flow properties. These modifications also allow measurements of air flow characteristics with greater precision. A CFD-based approach is utilized for the design of the intake section and fan. Steady-state simulations are performed, and the rotor-stator interaction is handled with the frozen rotor and mixing plane approaches. The numerical and experimental results are compared, to validate the results of all applied methods.

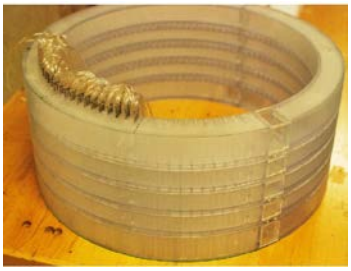

(a) (b)

Fig. 3 (a) Rotor without the exchangeable fan. (b) Stator

2. Generator Model Specifications

The geometry used in the present work is based on the electric generator model studied by Moradnia et al. [11]. This generator model has a rotor with 12 poles, a fan attached on top of the rotor, 4 rows of stator cooling channels along the axis of rotation, see Fig. 2. Each row includes 108 ventilation channels and 108 winding coils. The stator height is *0.175m*. The rotor tip radius and the stator inner and outer radii are *0.178m*, *0.1825m* and *0.219m*, respectively. The height of the stator ventilation channels is *4.7mm*. The rotational speed of the rotor is *2000rpm* to preserve the Reynolds number of the original electric generator [13], yielding a rotor tip speed of *37m/s*. The rotor and fan rotate in the counter-clockwise direction, looking from above. The air flow is driven exclusively by the rotor rotation, with its co-rotating fan.

The experimental rig is exclusively designed and manufactured for detailed measurements of the flow of cooling air, and is also adapted for Particle Image Velocimetry (PIV) and pressure measurements. The geometry of the rotor and stator are slightly simplified with the purpose of improving the accuracy of the experimental results, and for preparing for the high-quality CFD simulations. The rotor and stator are manufactured using rapid prototyping methods. The rotor, see Fig. 3(a), is manufactured using a Stereo Laser Sintering (SLS) process, since it has to withstand large centrifugal forces. The stator, see Fig. 3(b), is manufactured using a Stereo Lithography Apparatus (SLA) process as it has better surface finish, lower tolerance and higher accuracy.

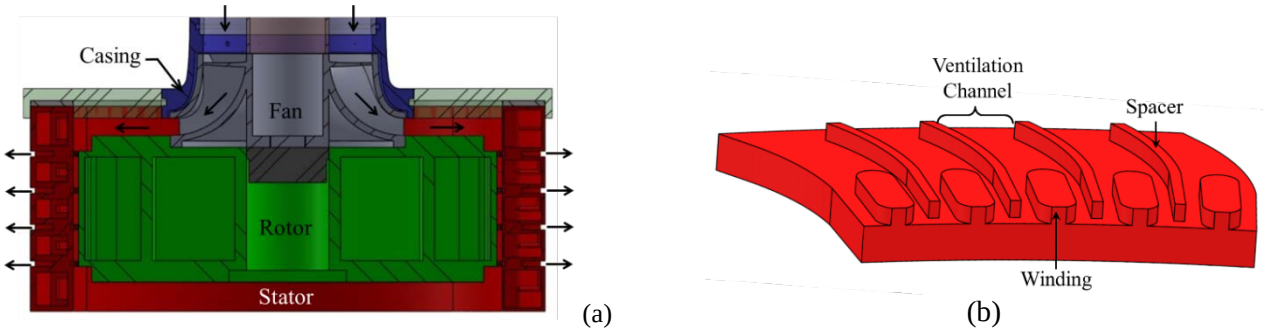

Fig. 4 (a) Cross-section of the generator model. (b) Sector of stator with ventilation channels.

Figure 4 shows a cross-section of the generator model, and a close-up of the stator channels. The generator used in this work is axially cooled, i.e. the flow of cooling air is axial in the air gap and in the inter-polar space. Figure 4(a) shows that the air enters the machine through the fan at the top, and leaves the machine radially, through the stator channels. The bottom is closed. The same geometry is used in the numerical simulations. The number of stator cooling channels and coils in each row (108) is divisible by the number of rotor poles and fan blades (12). The computational domain can thus be reduced to a 1/12th sector in the tangential direction, including 9 cooling channels in each channel row, one rotor pole and one fan blade passage, while employing cyclic boundary conditions at the sides of the domain.

Morania et al. [11] showed that flow separations at the inlet baffles and fan blade trailing edges, and a recirculation at the inlet region of the original generator model, had negative impacts on both the experimental investigations and the numerical simulations. It was also not possible to make a direct measurement of the flow rate through the machine. The PIV measurements inside the channels of the original model, by Hartono et al. [16], showed that a recirculation consumed half the channel width. This was caused by an insufficient flow rate due to the excessive losses at the inlet and in the fan. The present work addresses all these shortcomings, and significantly improves the ventilation design of the model as well as both the experimental and numerical accuracy.

2.1 Intake Design

The intake is in the present work designed to give a controlled inlet velocity distribution with losses as low as possible, and to facilitate accurate flow rate measurements. It consists of two concentric pipes, a bell-mouth at the inlet and a nose cone on top of the inner pipe, see Fig. 5. The bell-mouth and the nose cone are manufactured using PolyJet 3D printing with a rigid opaque material which leads to smooth surfaces and high axisymmetric precision. They are attached to Plexiglas pipes and fixed by O-rings to make a contiguous surface. The inner radius of the outer pipe (R2) is *0.072m* and the outer radius of the inner pipe (R1) is *0.035m*. The pipes are fixed to each other by 3D printed airfoil-shape spacers to make sure that they are concentric. These airfoil-shape spacers also ensure that the flow disturbance and blockage are as low as possible.

A bell-mouth is usually used when an inlet is positioned in a large reservoir or supply source. The reservoir can be an outside ambient, room or plenum chamber. A good design of a bell-mouth entry ensures that the flow is uniform and the loss induced at inlet is minimized. A bell-mouth inlet can increase the flow rate and reduce the noise, turbulence and pressure drop [17]. The bell-mouth inlet can be referred to as a nozzle with zero β ratio, which is the ratio between its throat diameter to the reservoir diameter. Its geometry typically consists of a smooth convergent inlet followed by a constant throat area. The convergent part here has an elliptical profile recommended in *ASME MFC-26* [18]. The nose cone on the inner pipe act as an obstruction in the flow stream, see Fig. 5. It changes the velocity and pressure of the flow gradually like a contraction cone. This part works as differential pressure type flowmeter device. It allows a determination of the mean velocity and the volume flow rate from the differential static pressure acquired from two wall taps located on the wall of the outer pipe, at positions 1 and 2, see Fig. 5. An elliptic profile is used for the nose cone. This shape is advantageous for subsonic flows due to its blunt nose and tangent base. The full body of revolution of the nose cone is formed by rotating the profile around the centerline. The fineness ratio of *2.0* is used for its design. The fineness ratio is the ratio of the length of a nose cone compared to its base diameter.

The computational domain of the intake simulations is shown in Fig. 6(a). It is simulated as a 2D axisymmetric case. The steady-state numerical simulations are done using the FOAM-extend CFD toolbox. The volume flow rate is set at the inlet and a constant pressure is set at the outlet. The e $\overline{v^2} - f$ low Reynolds RANS turbulence model is used. This model solves the turbulent kinetic energy, k, and dissipation, ε, with additional equations for the wall-normal turbulence stress, v^2, and elliptic relaxation function, f. The model includes the near-wall turbulence anisotropy as well as the non-local pressure-strain effects [18]. The y^+ value is lower than 1 at all walls. The second-order accurate linear upwind differencing scheme is used for the discretization of the convection term in the momentum equation. Figure 6(a) shows the simulated velocity contour in the intake section, which gradually increases due to the contraction. Importantly, there is no separation during the velocity increase process.

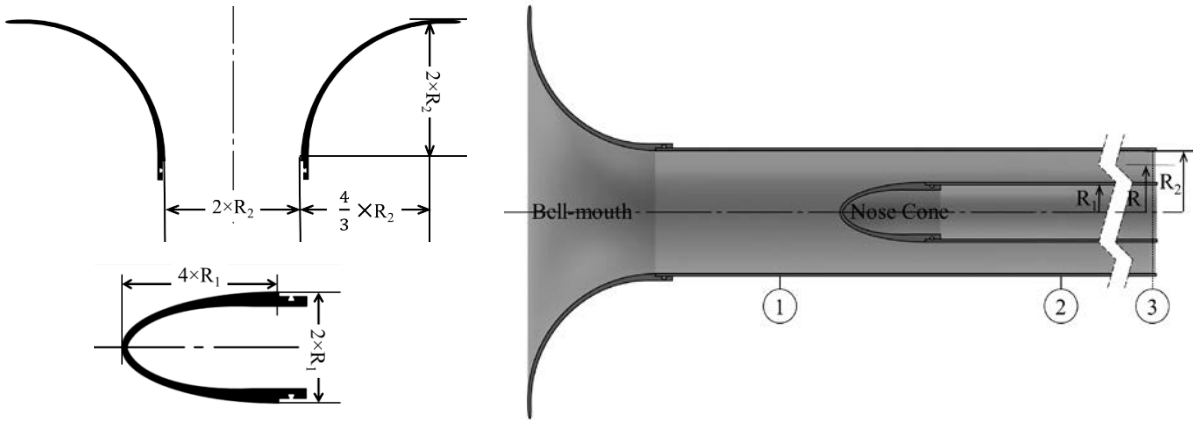

Fig. 5 The intake. Static pressure is measured at positions 1 and 2. The velocity is measured across line 3.

The volume flow rate and the square root of the static pressure difference between points 1 and 2 are proportional to each other according to

$$Q \propto \sqrt{\Delta P/\rho}. \quad (1)$$

Knowing the proportionality coefficient, the flow rate can be computed by measuring the pressure difference. The proportionality coefficient is determined using the CFD results. A range of inlet flow rates are simulated, to determine the corresponding pressure differences. A curve is fitted to the simulated results in Fig. 6(b), from which the proportionality coefficient can be determined. Experimental measurements are done to check the accuracy of the numerical data. The pressure difference and the velocity distribution are measured by a manometer and a five-hole probe, respectively. The velocity is measured across the annulus upstream the fan, along line 3 in Fig. 5. A comparison of the numerical and experimental velocity profiles is shown in Fig. 6(c), where the values are normalized by the bulk velocity, U_b. There is an excellent agreement between the numerical and experimental results. These profiles are taken at a rotor rotational speed of *2000rpm*, yielding a flow rate of about *0.15m^3/s*.

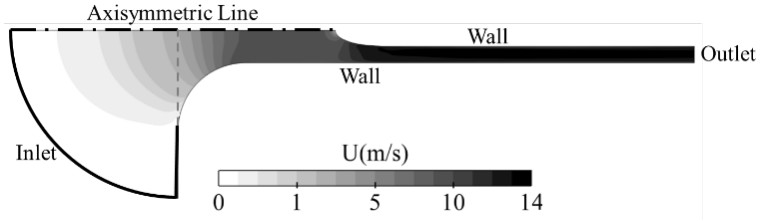

(a)

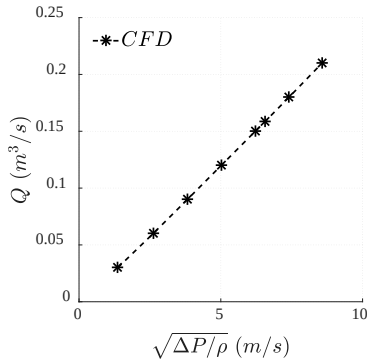

(b)

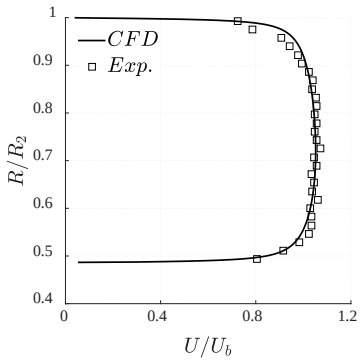

(c)

Fig. 6 (a) Velocity contours for inlet flow rate *0.15m^3/s*. (b) Flow rate as a function of square root of pressure difference. (c) CFD vs. experimental normalized velocity profiles at the end of intake section at *2000 rpm*.

Additional velocity and pressure difference investigations are done at different rotational speeds. The bulk velocities of the numerical predictions and experimental measurements are compared in Fig. 7(a), as a function of the square root of the pressure difference. It is shown that the flow rate measurement technique is reliable in the entire range of operation. The experimental relation between the rotational speed, the pressure difference, and the flow rate is presented in Fig. 7(b). It is the characteristic curve of the generator based on the measured static pressure difference in the intake. There is a linear relation between the rotor speed and the flow rate into the generator.

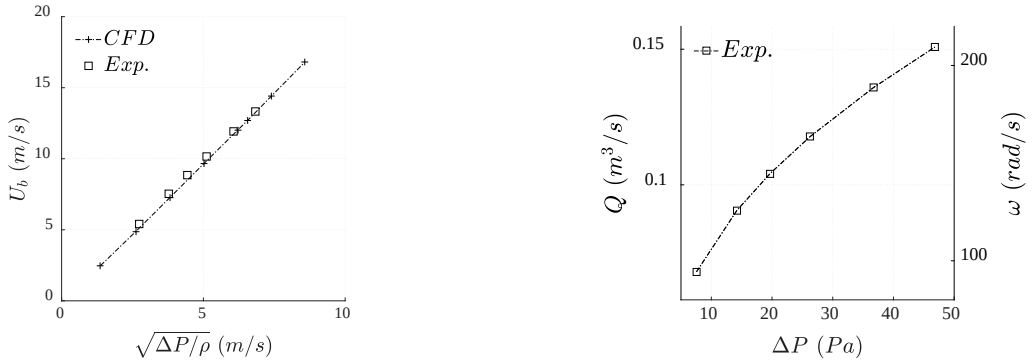

(a) (b)

Fig. 7 (a) Bulk velocity as a function of square root of pressure difference. (b) The relation between rotational speed, pressure difference and flow rate.

2.2 Fan Design

A new fan is designed in the present work, see Fig. 8. It resolves the aforementioned disadvantages of the original fan and has better aerodynamic characteristics. The previous fan was a semi-closed impeller with simple radial blades. The new fan has a shrouded closed impeller. The main dimensions of the new fan are restricted to the existing rig, such as the trailing edge tip radius and the impeller eye width. The design process of the impeller of the new fan consists of two main steps; generation of the flow passage and evaluation of the inlet and outlet blade angles. The flow passage generation mainly includes the calculation of the hub and shroud profiles. The hub and shroud profiles are designed based on guidelines provided in [20-22]. These profiles make sure that the flow in the impeller undergoes a gradual deflection in the axial-radial plane, leading to a change in flow direction from axial to radial. The leading edge blade angles are computed based on a velocity triangle consisting of the absolute velocity (c_1), the blade circumferential velocity (u_1), and the relative velocity (w_1). The fan inlet velocity triangle is depicted in Fig. 8(b). The absolute velocity is assumed to be constant and purely axial, with a magnitude determined by an iterative CFD process. The blade circumferential velocity is set by the required rotational speed. It increases linearly from hub to shroud, due to the solid-body rotation, and consequently leads to a varying relative flow angle (β_1). The leading edge blade angle is designed to align with the relative flow angle, which minimizes flow separation and gives a higher fan efficiency. The blades are purely radial at the trailing edge, since the air flow leaves into a region where the rotor poles have the same rotational speed as the fan.

CFD simulations are used in the fan design process, using the steady-state single rotating reference frame (SRF) modeling in FOAM-extend. A 1/12 sector of the fan, i.e. one blade passage, is simulated and the blades are assumed infinitely thin. This CFD-based design process assures that the fan can handle the change of axial flow to radial flow, and the pressure build-up, without separation. The final design is manufactured using PolyJet 3D printing, as precision and surface smoothness is important in the fan.

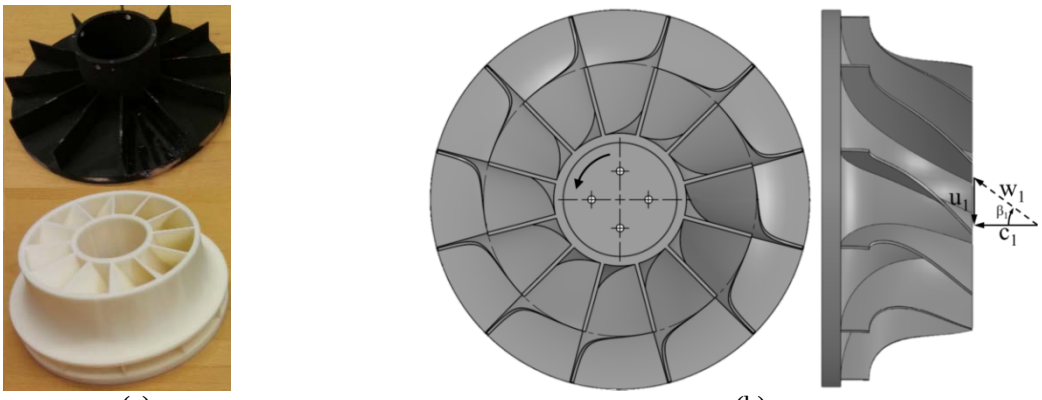

(a) (b)

Fig. 8 (a) Original fan (top) vs. modified fan (bottom). (b) Modified fan with removed shroud.

The simulated pressure contours on the pressure and suction side of the fan blades, and on the hub and shroud, are shown in Fig. 9(a). The pressure gradually increases from the leading edge to the trailing edge of blades. To finally check the effect of the new fan on the volume flow rate in the generator, the inlet velocity profiles are measured with and without the fan blades, see Fig. 9(b). In the case of the fan without blades, the geometry is identical to the fan with blades but there are no blades, so it only includes hub and shroud. The shroud is stationary, connected to the body of the generator and the hub is connected to the rotating rotor. The inlet flow rate is more than doubled when the fan with blades is applied.

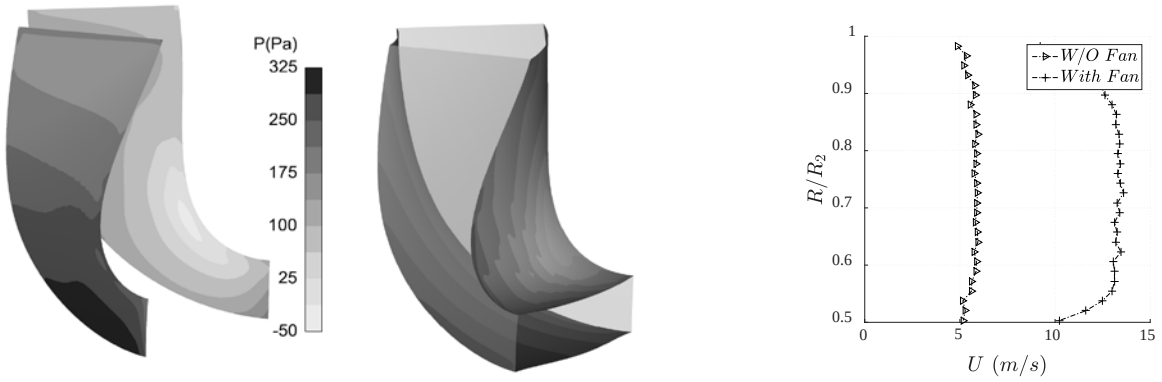

(a) (b)

Fig. 9 (a) Pressure on fan blades, and on hub and shroud. (b). Velocity comparison with and without fan blades, measured at *2000rpm*.

3. Numerical Modelling of the Entire Generator Model

The numerical simulations of the entire generator model are performed using the FOAM-extend CFD tool, and the steady-state multiple reference frame (MRF) method. The MRF method does not rotate any part of the mesh, but applies source terms in the momentum equations for the rotation. The MRF method requires that stationary and rotating zones are defined, separated from each other by axisymmetric interfaces, see Fig. 10(a). Two different approaches are used to handle the rotor-stator interaction (RSI), frozen rotor (FR) and mixing plane (MP). The frozen rotor approach retains the relative position of the rotor and stator and thus transfers the flow parameters in fixed positions. The mixing plane method averages the flow parameters in the circumferential direction and transfers the averaged values to the adjacent interface. The relative position between the rotating and stationary parts is thus not taken into account in the mixing plane approach.

A low-Re turbulence model is required for modeling the effects of turbulence, due to the relatively low velocities and small dimensions in the stator channels. The Launder-Sharma $k-\varepsilon$ turbulence model is used in the present study. The mesh is generated using the *ANSYS ICEM CFD* mesh generator, keeping the wall y^+ values at about 1. The mesh is block-structured, covering a 1/12 sector in the tangential direction, employing cyclic boundary conditions on the two sides, see Fig. 10. The computational domain hence includes one rotor pole, one fan blade passage, four stator cooling channel rows and nine cooling channels in each channel row. The results are considered converged when the residuals are small and stabilized, at the same time as the rotor axial torque is stabilized.

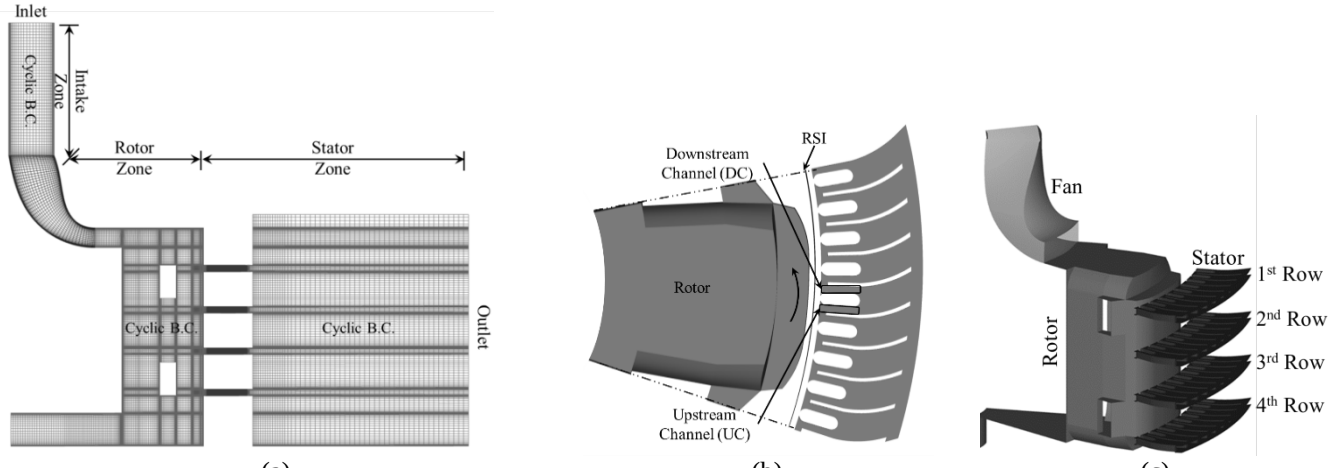

(a) (b) (c)

Fig. 10 Computational domain and MRF zones. Inlet, outlet and cyclic boundary conditions are illustrated.

4. Experimental Setup

The experimental part of this work includes velocity measurements at the inlet of the fan and total pressure measurements at the outlet of the stator channels. The velocity measurements at the inlet are performed using the five-hole pressure probe shown in Fig. 11(a). The probe is of L-type with a tip diameter of *1.6mm*. The probe is calibrated for cone angles from 0 to 52 degree. The measurement accuracy is better than *1%* for the velocity magnitude and 0.5^o for the flow angles. A one-axis traversing system with an accuracy of *100μm* is used to position the 5-hole probe at the generator inlet. The time-mean statistics are evaluated from 2000 samples, from which the velocity is calculated. The outlet measurements are performed using a total pressure probe rake. It is traversed by a three axis system, which

covers all the ventilation channels, as shown in Fig. 11(b).

The 14 tubes in the rake capture the total pressure distribution at the stator channel outlets, see Fig. 12. The tubes are aligned with the main flow direction, to optimize the measurement accuracy. The outlet total pressure is averaged over 1000 data samples using a scanning frequency of *500Hz*, corresponding to about 67 rotor rotations. The values are monitored using a 16-channel *PSI 9116* digital pressure scanner from *Pressure Systems Inc*. The measuring range of the scanner transducers is *±2500Pa*. To maintain the highest possible accuracy in a low-pressure range, the pressure transducers are regularly reset to zero before each set of measurements. The resulting precision of the transducer offset is better than *0.2Pa*. The statistical uncertainty of the mean total pressure is *0.06Pa*, with 99% confidence in regions with the largest pressure fluctuations.

(a) (b)

Fig. 11 (a) 5-hole pressure probe on a one-axis traversing system, (b) Total pressure rake on a three-axis traversing system.

5. Results

Figure 12 shows a comparison between the experimental and numerical total pressure, P_{tot}, from one spacer to the adjacent spacer in the direction of the runner rotation along the throat width, X_t. The experimental total pressure presented here is the average of the total pressure measured in 100 successive channels in each row of the stator. The bars on the experimental curve present the standard deviation of the measurements. The numerical total pressure presented in Fig. 12 is for the frozen rotor approach, averaged over the nine stator channels of each row. For the mixing plane approach there is no difference between the flows in the different channels of each row, so the total pressure of the middle channel of each row is depicted. In the first and second row the numerical total pressure is a bit higher than the experimental data, and in the third and fourth row it is slightly lower. The comparison shows that the numerical results are very similar to the experimental data, and that the frozen rotor and mixing plane approaches give similar results. The total pressure distributions are not symmetric across the channels. The peak is at the upstream side of the outlet.

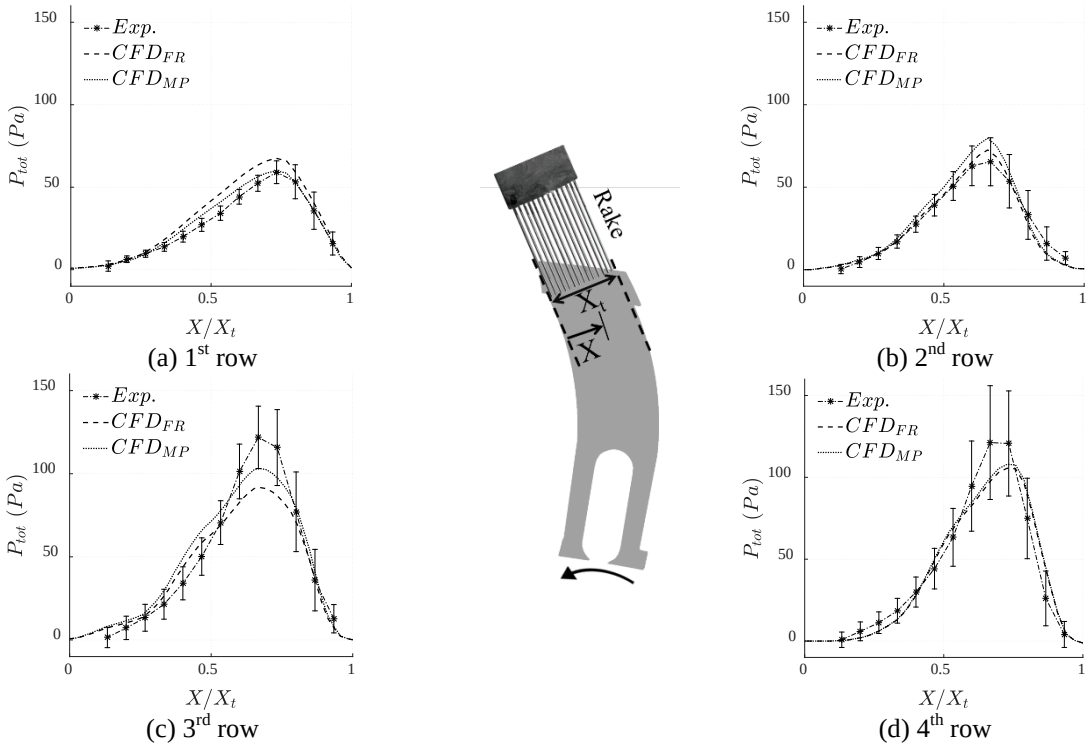

(a) 1st row (b) 2nd row

(c) 3rd row (d) 4th row

Fig. 12 Experimental and numerical averaged total pressure at the outlet of the stator channel rows.

Figure 13 shows areas of numerically predicted reverse radial flow in the stator channels. All channels have a positive radial flow at both sides of the coils and reversed flow in the wakes of the coils. There is a small separation at the tangentially downstream side of the spacer leading edges, and at some of the coils. The effect of the two different rotor stator coupling approaches is also shown. The result of the mixing plane simulation is similar in all channels, as expected. In the results of the frozen rotor simulation, the fixed relative position of the rotor with respect to the stator results in different flow fields in different channels. This is especially due to the non-axisymmetric rotor geometry, such as the inter-polar spaces. Overall, the reverse flow regions are smaller in the 1st and 2nd row compare to the 3rd and 4th row. This difference is due to a relatively larger axial velocity component at the entrance to the 1st and 2nd rows whereas the tangential component is larger at the entrance to the 2nd and 3rd rows. The flow distribution dissimilarity is expected to be larger when the tangential component of the velocity at the inlet of the stator channel is larger.

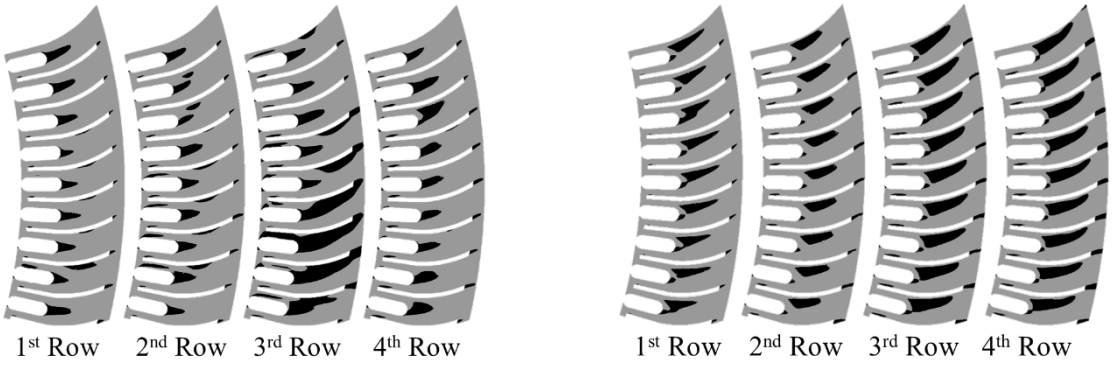

Fig. 13 Areas of reverse radial flow (dark). Left: Frozen Rotor. Right: Mixing Plane

Figure 14(a) shows how the total flow through each ventilation channel, Q_t, is distributed between the two sides of the winding, i.e. the upstream channel (UC) and the downstream channel (DC) (see Fig. 10(b)). The results are presented for both the frozen rotor and mixing plane approaches. For the frozen rotor approach the flow rate is averaged over all nine channels of each row, while the center channel is used for the mixing plane results. In all rows there is more flow in the upstream channel compared to the downstream channel. A good design should distribute the cooling air as evenly as possible between the channels, and also inside each channel, which shows that there is room for improvement in the current generator design. Figure 14(b) compares how the total flow rate, Q_T, is distributed between the stator channel rows. The experimental flow rate for each row is estimated from the measured total pressure at the outlet of the stator channels. The flow is distributed quite evenly between the rows, with a tendency to increase from row 1 to row 4. The prediction using the mixing plane approach is slightly closer to the experimental results, except for the second row.

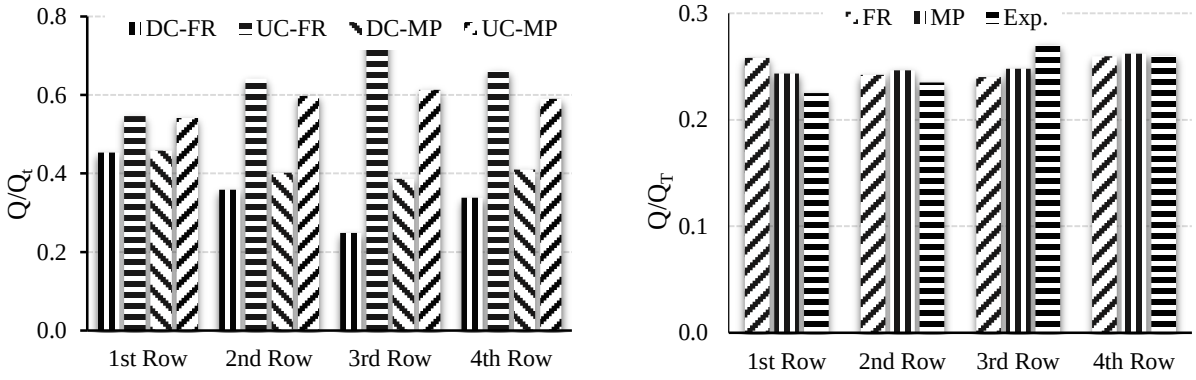

Fig. 14 (a) Distribution of total flow at upstream and downstream sides of the stator winding. (b) Distribution of total flow between channel rows

6. Conclusions

An existing experimental generator ventilation model is modified to increase the flow rate and to improve the flow behavior. CFD is used in the design process. The flow of cooling air is experimentally studied using 5-hole probe measurements at the inlet and total pressure rake measurements at the outlet of the stator channels. The new intake design gives an inlet velocity that is evenly distributed, and makes it possible to do direct measurements of the flow

rate. The new fan doubles the flow rate compared with a case without the fan blades, and gives a more evenly distributed flow into the rotor.

The experimental data is used to validate numerical simulations of the flow field. The simulations are performed using the steady-state multiple references frame method with the frozen rotor and the mixing plane rotor-stator coupling approaches. The investigations are done under cold conditions, since the present focus is restricted to the characteristics of the flow of ventilation flow inside electric generators, and numerical techniques for its accurate prediction. The numerically predicted flow features agree very well with the experimental results at all experimental sections, and the numerical approach may be considered useful for developing a better understanding of the flow of cooling air in electric generators.

The flow is not evenly distributed through the different channel rows, and inside each channel. There is more flow at the upstream side of the windings, which suggests that there is still room for improvement of the stator channel inlet design.

Acknowledgments

The research presented was carried out as a part of the "Swedish Hydropower Centre - SVC". SVC has been established by the Swedish Energy Agency, Energiforsk and Svenska Kraftnät together with Luleå University of Technology, The Royal Institute of Technology, Chalmers University of Technology and Uppsala University. www.svc.nu. The simulations were performed on resources provided by the Swedish National Infrastructure for Computing (SNIC) at C^3SE and NSC.

References

[1] Traxler-Samek G., Zickermann, R. and Schwery, A., 2010, Cooling Airflow, Losses, and Temperatures in Large Air-Cooled Synchronous Machines, Industrial Electronics, IEEE Transactions on , vol.57, no.1, pp.172-180.

[2] Boglietti A., Cavagnino A., Staton D., Shanel M., Mueller M. and Mejuto C., 2009, Evolution and modern approaches for thermal analysis of electrical machines, Industrial Electronics IEEE Transactions, vol.56, pp. 871-882.

[3] Pickering S. J., Lampard D. and Shanel M., 2001, Modelling ventilation and cooling of the rotors of salient pole machines, International Electric Machines and Drives Conference IEMDC 2001 IEEE pp. 806-808.

[4] Shanel M., Pickering S.J. and Lampard, 2003, Conjugate heat transfer analysis of a salient pole rotor in an air cooled synchronous generator, International Conference of Machines and Drives IEEE vol.2 pp. 737-741.

[5] Ujiie, R. and Arlitt, R. and Etoh, H, 2006, Application of Computational Fluid Dynamics (CFD) on Ventilation-Cooling Optimization of Electrical Machines, Review Energy Technologies - generation, transmission and distribution of electric and thermal energy (ICEMENERG), pp. 17-22.

[6] Traxler-Samek G., Zickermann R. and Schwery A., 2008, Advanced calculation of temperature rises in large air-cooled hydro-generators, International Conference on Electrical Machines (ICEM) vol. 1 pp. 1-6.

[7] Toussaint K., Torriano F., Morissette J. F., Hudon C. and Reggio M., 2011, CFD analysis of ventilation flow for a scale model hydrogenerator, ASME Power Conference collocated with JSME ICOPE 2011 pp. 627-637.

[8] Pasha A. A., Hussain M. and Gunubushanam N., 2010, Experimental and CFD analysis of hydrogenerator, stator Proc. of the 37th National & 4th Int. Conf. on Fluid Mechanics and Fluid Power, India.

[9] Schrittwieser M., Marn A., Farnleitner E. and Kastner G., 2012, Numerical analysis of heat transfer and flow of stator duct models, International Conference on Electrical Machines (ICEM), pp. 385-390.

[10] Zhang Q. F., Yan J. L., Wang M. and Chen Z. X., 2012, CFD Application on Ventilation System of Hydro-generator, Advanced Materials Research, vol. 383, pp. 3561-65.

[11] Moradnia P., Golubev M., Chernoray V. and Nilsson H. 2014 Flow of cooling air in an electric generator model– An experimental and numerical study, Journal of Applied Energy vol. 114, pp. 644-653.

[12] Moradnia P., Chernoray V. and Nilsson H., 2014, Experimental assessment of a fully predictive CFD approach, for flow of cooling air in an electric generator, Journal of Applied Energy vol. 124, pp. 223-230.

[13] Moradnia P., Chernoray V. and Nilsson H., 2011, Experimental and numerical investigation of the cooling air flow in an electric generator, HEFAT 2011 8th Int. Conf. on Heat Transfer, Fluid Mechanics and

Thermodynamics pp. 242-249.

[14] Klomberg S., Farnleitner E., Kastner G. and Biro, O., 2014, Comparison of CFD analyzing strategies for hydro generators, International Conference of Electrical Machines (ICEM), pp. 1990-1995.

[15] Klomberg S., Farnleitner E., Kastner G. and Biro O., 2014, Implementation of a new simulation strategy for a cooling study of large hydro generators, International Conference Power Electronics, Machines and Drives (PEMD), pp. 1-6.

[16] Hartono E., Golubev M., Moradnia P., Chernoray V. and Nilsson H., 2012, PIV Measurement of Air Flow in a Hydro Power Generator Model, 16th Int Symp on Applications of Laser Techniques to Fluid Mechanics, Lisbon, Portugal.

[17] Dhongadi M. M., Rao K. S., Srinivas G. R., and Prakas C. P. S., 2013, Computational Fluid Dynamics Simulation and Optimization of a Gas Turbine Inlet Duct, International Journal of Engineering Research and Technology Vol. 2, No. 9.

[18] ASME MFC-26 2011, Measurement of Gas Flow by Bellmouth Inlet Flowmeters, ISBN: 9780791833551

[19] Davidson L, Nielsen P, and Svenningsson A., 2003, Modifications of the v2-f model for computing the flow in a 3D wall jet, Turbulence, Heat and Mass Transfer vol. 4, pp. 577-584

[20] Stockman N. O. and Kramer, J. L., 1963, Method for design of pump impellers using a high-speed digital computer. National Aeronautics and Space Administration.

[21] Stanitz J. D. and Prian, V. D., 1951, A Rapid Approximate Method for Determining Velocity Distribution of Impeller Blades of Centrifugal Compressors, National Advisory Committee for Aeronautics.

[22] Milos Teodor, 2012, Impeller Design Using CAD Techniques and Conformal Mapping Method, Centrifugal Pumps, Dr. Dimitris Papantonis (Ed.), ISBN: 978-953-51-0051-5.